Eur. Phys. J. A **20**, 15–29 (2004)
DOI 10.1140/epja/i2002-10313-4

THE EUROPEAN PHYSICAL JOURNAL A

Hyperdeformed and megadeformed nuclei

Lessons from the slow progress and emerging new strategies

J. Dudek[1,a], K. Pomorski[2], N. Schunck[3], and N. Dubray[1]

[1] Institut de Recherches Subatomiques, IN2P3-CNRS/Université Louis Pasteur, F-67037 Strasbourg Cedex 2, France
[2] Katedra Fizyki Teoretycznej, Uniwersytet Marii Curie-Skłodowskiej, PL-20031 Lublin, Poland
[3] Department of Physics, University of Surrey, Guildford GU2 1XH, UK

Received: 19 December 2002 /
Published online: 24 February 2004 –

Abstract. We discuss physics motivations related to hyperdeformed nuclei and more generally large nuclear deformations at high angular momenta. Possible reasons for the experimental difficulties encountered so far are discussed together with suggestions related to the new setting of priorities that combine our present-day knowledge about the behavior of hot nuclei, in particular, the Jacobi transitions, and the hyperdeformed-shell structures.

PACS. 21.60.-n Nuclear structure models and methods – 21.90.+f Other topics in nuclear structure

1 Introduction

Large-scale microscopic calculations of the nuclear potential energy surfaces predicted systematically the existence of superdeformed and hyperdeformed configurations at high angular momenta. The existence in nature of the high-spin nuclear *superdeformation* has been in the meantime well established experimentally in terms of discrete transitions and hundreds of superdeformed bands have been observed in nuclei in various mass ranges beginning with relatively light ones, $A \sim 40$, through medium heavy, $A \sim 80$, $A \sim 130$ and $A \sim 150$, up to the heaviest ones, mercury range, $A \sim 180$. The very large deformations associated with the so-called secondary minima in the actinide nuclei have been known for many years before the first superdeformed band in the ^{152}Dy nucleus [1] had been observed in 1986 (cf. fig. 1).

The high-spin hyperdeformed discrete nuclear states have never been seen so far in experiment although the corresponding theoretical predictions have been obtained within the same formalism that was successful in predicting and interpreting the superdeformed structures. In particular, already in 1987, *i.e.* when just a few superdeformed nuclei were known experimentally it has been recognized [2] that the *pseudo-SU_3 symmetry* of the nuclear mean field implies the existence of the whole *abundance scheme* for nuclear superdeformation. The experimental results known today confirm to the full extent the systematic appearance of the superdeformed-shell closures implied by the pseudo-SU_3 symmetry of the mean field, figs. 1 and 2 in the above reference. (For earlier reviews related to superdeformation cf., *e.g.*, refs. [3–5]; for the early discussion related to nuclear stability in terms of the harmonic-oscillator properties —ref. [6]. For an extensive survey of the present-day information about nuclear superdeformation the reader is referred to the compilation [7] where both an overview of the experimental results as well as an extensive list of the published articles on the subject can be found.) More precisely, introducing the main-shell quantum number N and the related (pseudo-SU_3) quantum numbers $\tilde{N} = N - 1$ and $\tilde{n}_z = n_z$, where $\tilde{n}_z = 0, 1, \ldots \tilde{N}$, one can easily recognize in any realistic nuclear mean-field spectra the characteristic pattern of mutually crossing multiplets. An approximate pseudo-SU_3 symmetry implies approximate $(2s+1)$ $(\tilde{N} - \tilde{n}_z + 1)$ degeneracies in the single-particle energies that produce in turn a characteristic pattern of increased level-density areas separated by the low level-density areas (gaps) and provide an excellent parameterisation of the today known abundance of the nuclear high-spin superdeformation (cf., *e.g.*, figs. 1 and 2 in ref. [2] and references therein).

2 Fifteen years of superdeformation studies

Before discussing in more detail the physics motivation and expected research directions related to the *hyperdeformation*, let us try to summarize briefly what appears to represent the most important achievements in the *superdeformation* studies. Of course, there is no place here to overview the evolution that lead to our present-day understanding of superdeformed nuclei. The reader is referred to other publications on the subject, *e.g.*, those cited in

[a] e-mail: Jerzy.Dudek@IReS.in2p3.fr

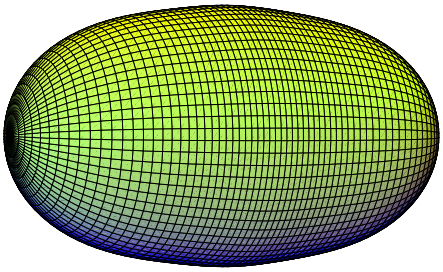

Fig. 1. The superdeformed nucleus ^{152}Dy, according to the measurements of ref. [8] has the quadrupole moment $Q_2 = 17.2$ eb. The corresponding deformation $\alpha_{20} = 0.61$ and $\alpha_{40} = 0.11$ obtained, *e.g.*, from the calculations with the Woods-Saxon potential as in ref. [9] reproduces the measured dynamical moments and the quadrupole moment. The shape presented in the figure corresponds to the above deformation.

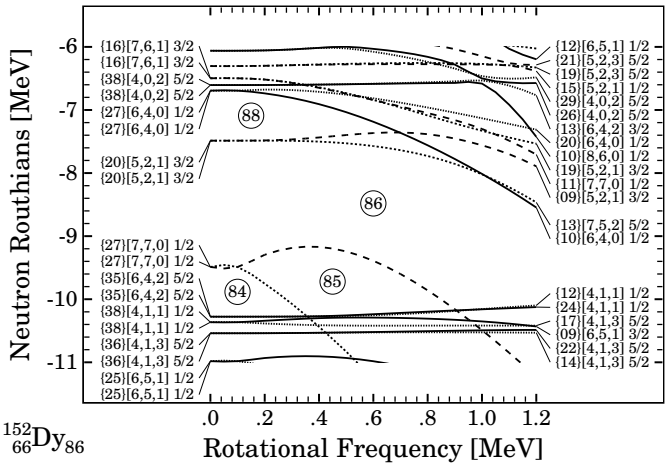

Fig. 2. The neutron single-particle levels as a function of the rotational frequency. The results correspond to the superdeformed nucleus ^{152}Dy at the equilibrium deformation calculated using the deformed Woods-Saxon potential. The numbers in curly brackets give the percentages of validity of the attached Nilsson labels.

the introduction. Below, just a few selected aspects will be mentioned that we consider particularly relevant also in the hyperdeformation context.

2.1 Realistic mean fields are not harmonic oscillators

Let us begin by recalling first these expectations that the superdeformation studies *did not* confirm. First of all, the realistic calculations such as deformed Woods-Saxon, self-consistent Hartree-Fock or Relativistic-Mean-Field models show repeatedly the non-applicability of the harmonic-oscillator approximation in the analyses of the large deformation, especially at high spins. Such a conclusion can be drawn when analyzing the structure of the single-nucleonic wave functions in terms of the deformed harmonic-oscillator basis

$$\psi^{(n)}(\boldsymbol{r}) = \sum_{N,n_z,\ell_z,s_z} a^{(n)}_{N,n_z,\ell_z,s_z} \varphi_{N,n_z,\ell_z,s_z}(\boldsymbol{r}), \qquad (1)$$

where $\psi^{(n)}(\boldsymbol{r})$ denotes a realistic nucleonic wave function in the deformed potential and $\varphi_{N,n_z,\ell_z,s_z}(\boldsymbol{r})$ the deformed harmonic-oscillator basis wave function.

In fig. 2 we represent the typical single-particle Routhian spectrum (here for the neutrons). The numbers in curly brackets give the percentage of the leading Nilsson label in the corresponding wave function (the maximum amplitude squared, $|a^{(n)}_{N,n_z,\ell_z,s_z}|^2$). The deformation chosen is close to the calculated equilibrium deformation as obtained with various models for the superdeformed ^{152}Dy nucleus (cf., *e.g.*, refs. [9,10]). One can see from the right-hand side of the figure, corresponding to the large-frequency limit, that over a half of the levels have the maximum Nilsson amplitude that does not exceed 15%, while the other half does not exceed 25%. Let us recall at this point that the harmonic-oscillator basis is forced to deform in such a way that an optimum spatial overlap between the basis potential and the studied potential is achieved. In other words, the discussed small overlap between the realistic wave functions and the harmonic-oscillator basis wave functions is not related to the *sphericity* of h.o. basis, but rather reflects large structural differences between the wave functions calculated with these two potentials, much larger than what has been discussed so far.

As a result, since one should not expect any significant overlap between the deformed harmonic oscillator and the realistic-model wave functions at high spins and large deformations, important deviations between the harmonic-oscillator–based predictions and those of the realistic models are to be expected. A particular consequence of that fact is given as an example in the following section.

2.2 Inapplicability of the "2 : 1 Axis Ratio Criterion"

We often used to quote statements such as "the axis ratio corresponding to a given superdeformed nucleus is close to 2 : 1". Those statements are *not* confirmed by experiment and are probably incorrect as commented below.

The microscopic calculations successfully predicting as well as interpreting the detailed structure of the superdeformed bands involve obviously the corresponding equilibrium deformations (that may in general (slightly) vary with spin). Similarly, the calculated multipole moments depend in a rather sensitive manner on the equilibrium deformations used, especially the quadrupole one. For instance, the experimental result for the average quadrupole moment in the superdeformed band in ^{152}Dy, $Q_t = 17.5(2)$ eb, ref. [8], is close to the microscopic calculation results at the equilibrium deformation of $\alpha_{20} \sim 0.61$ and $\alpha_{40} \sim 0.1$. The corresponding ratio of the semi-axes is

$$R_z/R_x = 1.72 \ \text{ (compare: } \sqrt{\pi} = 1.772), \qquad (2)$$

and if anything, it is closer to $\sqrt{\pi}$ than to 2. In the mass range $A \sim 130$ this geometrical axis ratio is even smaller: $R_z/R_x = 1.45$ (compared to $\sqrt{2} \sim 1.414$). Of course both numbers ($\sqrt{2}$ and $\sqrt{\pi}$) are cited here to emphasize a huge

discrepancy between the measurement-justified values and the (too often) incorrectly quoted ones.

Let us recall that according to one of the accepted criteria, a nuclear configuration is called superdeformed not so much according to the size of the observed axis ratio but rather according to structural features such as the presence (or not) of the intruder levels originating from the "$(N+2)'$-nd" main shell, where N denotes the principal shell quantum number at spherical shapes.

2.3 Pseudo-SU_3 symmetry and other discoveries

Despite the fact that the geometrical relations predicted by the harmonic pseudo-oscillator cannot be used in detailed analyses of experimental results, there remains a precious common factor in comparisons between the realistic nuclear mean-field calculations and the harmonic pseudo-oscillator potential: both obey (under certain limiting conditions) the pseudo-SU_3 symmetry[1]. As a consequence, the single-nucleon spectra resulting from the pseudo-oscillator and from a realistic Hamiltonian have similar degeneracy patterns as well as the clearly distinguishable correspondence of levels and energy gaps; however, the deformations at which analogous SD shell closures appear are different in both cases.

The harmonic oscillator obeys the SU_3 symmetry exactly, the pseudo-oscillator (cf. fig. 2 in ref. [2]) can be treated as a certain phenomenological realization of the SU_3 symmetry while the realistic mean-field Hamiltonians obey the symmetry only approximately. The usefulness of this symmetry concept can be appreciated from the prediction of *chains* (or series) of the SD gaps in the single-particle spectra that can be considered experimentally confirmed *today* but was not at all obvious when the symmetry concept was first introduced.

While the very existence and some properties of the superdeformed nuclei have been predicted by the theory (*e.g.*, the existence of the superdeformed-band structures in over a dozen of the rare-earth nuclei has been foreseen several years before their experimental discovery, ref. [11]), some special properties were not. That is in particular true in relation to the so-called "identical-band mechanism", ref. [12], and often discussed together with a mechanism of the "quantized angular momentum alignment". Here we are not going to discuss these aspects; the reader is referred, *e.g.*, to [5] (cf. also, *e.g.*, [13] and [14]).

Let us emphasize that a similar mechanism is expected in the hyperdeformed nuclei as well (the corresponding predictions are going to be published elsewhere).

Similarly, the additivity of the multipole moments was *a priori* not an evident aspect (for a related discussion cf., *e.g.*, ref. [10]).

[1] It is perhaps worth to remind that the adjective "pseudo" should not lead to any pejorative connotation. The so-called pseudo-SU_3 symmetry is from the point of view of mathematics just another physical realization of the SU_3 symmetry. This name has been introduced merely to distinguish between the physical realization of the SU_3 symmetry introduced earlier within the Elliot model and the one in the present context.

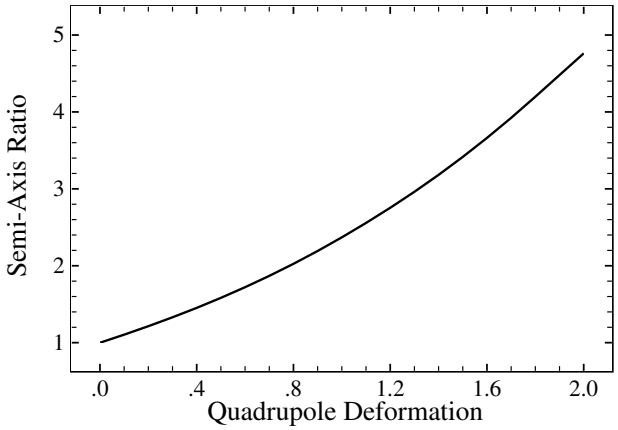

Fig. 3. Semi-axis ratio (longer-to-shorter) along the liquid-drop model minimum-energy path to fission for the ^{164}Er nucleus at spin zero. This curve can be seen as representing a typical relation for many nuclei.

3 Hyperdeformation: physics motivations

We are going to recall briefly what, in our opinion, represents an important physics motivation(s) for the hyperdeformation studies. Then, we will proceed to formulate a number of observations that have accumulated during the years of rather unsuccessful trying to observe the hyperdeformed nuclei in the discrete transitions. (For some earlier attempts in this experimentally very difficult domain, see ref. [15].)

3.1 Definition of a hyperdeformed nucleus

Let us begin by formulating some comments related to the very definition of the objects in question: how do we define a hyperdeformed nucleus or, in other words, when do we know that the hyperdeformation experiment has been successful?

For a long while the arguments based on the semi-axis ratios $a : b = 2 : 1$, for superdeformation, and $a : b = 3 : 1$ for the hyperdeformation have been commonly used. They were based on the expected analogies between the nuclear shell structure and that of the harmonic oscillator —expectations that contradict the results of the present-time experiments. Today we know, as recalled in the preceding section, that even with hundreds of large-deformation bands successfully identified, the "legendary" 2 : 1 axis ratio has most likely not been observed so far— and if so, then in a very few cases only.

In fig. 3 we show a typical semi-axis ratio curve valid for many medium heavy and heavy nuclei. In the center of the rare-earth region and in particular in the neighborhood of the ^{152}Dy nucleus the quadrupole deformations are typically of the order of $\alpha_{20} \sim 0.6$ or less; in the cerium and mercury regions, $A \sim 130$ and $A \sim 180$, respectively, the quadrupole deformations vary typically between 0.4 and 0.5. Consequently, in most of the nuclear configurations where the large deformations have been observed the semi-axis ratio varies between 1.5 to 1.7.

The "legendary" 3 : 1 axis ratio corresponds to $\alpha_{20} \sim 1.4$; if we use the liquid-drop model (for details see below) by calculating the total nuclear energy as a function of increasing α_{20} and letting several other deformations vary (usually up to the multipole order $\lambda \sim 16$ or more), we can obtain a reasonable estimate of other deformations, first of all α_{40}. At the quadrupole deformation as quoted above, the hexadecapole deformation may vary from 0.15 to 0.30 depending on the Z/N combination and on the actual spin, but without modifying the axis ratio in any important manner. What is commonly quoted in the literature as "hyperdeformation" corresponds very closely to $\alpha_{20} \sim 0.9$–1.0; this type of *hyperdeformed* nucleus would have *axis ratio 2 : 1* as seen from fig. 3.

We thus can conclude that the "geometry-based" criteria operating with the harmonic-oscillator properties turned out to be very restrictive, since even the ^{152}Dy superdeformed band would not qualify for its "noble" name.

Another, nuclear-structure–based "definition" of the hyperdeformation relies on the fact that the larger the elongation the lower the energies of the "exotic" orbitals that normally can be found only in the very high-lying spherical shells. Some authors prefer to use the corresponding criterion as less arbitrary: according to such a definition the observed nuclear configuration will be called hyperdeformed if there was at least one orbital occupied that originates from the corresponding $(N+3)'$-rd main shell when extrapolating to the nucleus's spherical shape.

Following rigorously this second criterion for the superdeformed shapes (in this case $(N+3) \rightarrow (N+2)$), many nuclei called today superdeformed would loose their characterizing adjective —we would need to call them just strongly deformed.

On the one hand, it should be emphasized that we are learning about many important, exotic properties of the nuclear behavior associated with the strongly elongated nuclei independently of the fact that they can/cannot be qualified according to one of the definitions cited above. On the other hand, the presence of the very exotic orbitals originating from $(N+n)$-th shells does bring a very important *particular* information about the very high-lying main shells; it may, *e.g.*, allow for energy level extrapolations into the continuum. The "definition" based on this mechanism is less vague; the two definitions are of course contradictory as discussed below.

3.2 Physics motivations

If found in nature, what will the hyperdeformed nuclei tell us, possibly new and exotic, about the nuclear behavior at the extreme conditions?

Since no single case has so far been observed in terms of the discrete lines at high angular momenta, several questions should be raised. First of all: the theoretical calculations that predicted and interpreted quite consistently a large body of experimentally known data related to superdeformation, predict at the same time the existence of much stronger-elongated shapes satisfying all the criteria that would allow them to be called hyperdeformed. Why should the transition: superdeformed $\rightarrow$ hyperdeformed cause so much more restrictive demand on the instrumental sensitivity so that no identification has been possible so far?

We believe that an important physical mechanism, related to the nuclear Jacobi transition [16] properties (see below) has been systematically "overlooked" in the past in many discussions related to searching for the hyperdeformation and selecting the cases for the experiments. Thus, it is not only the high instrumental sensitivity that is challenged but, at the present-day sensitivity, as we believe, the choice of the reaction should be much more restrictive. This will be discussed to a far extent below, so that here we rather turn to the question: Suppose one or more hyperdeformed nuclei have been identified, what should we (possibly) learn?

First of all the most evident: by measuring the hyperdeformation (defined in terms of the second, more precise definition of this term) we will be able to obtain very important information about the energy positions of the very high ($(N+3)'$-rd) shells. This in itself is surely an important achievement for high-precision future spectroscopic studies, yet in itself could be qualified as a standard item on the nuclear-structure agenda rather than "exotic" or "unusual".

A much more ambitious research program can be formulated in relation to the (pseudo) SU_3 symmetry in nuclei. Merely posing the very problem of existence or nonexistence of *a generally present nuclear symmetry*, even if only approximate, is in itself a fundamental-research question that is certainly worth addressing. The reader could have noticed that on the basis of the *superdeformation* studies we have considered this question positively answered: the (approximate) pseudo-SU_3 symmetry has been clearly confirmed by the discovery of the abundance scheme of the superdeformed nuclei as predicted earlier by theory. Why should hyperdeformation be any different?

It turns out that the shapes of most of the observed superdeformed nuclei can be considered relatively "compact". By enforcing more and more elongation, we will push the nuclei in question much closer towards fission/scission configurations thus encountering the configurations in which a certain "pre-identification" of the going-to-be fragments will become possible. *The pseudo-SU_3 structure of the nearly formed fragments cannot coexist with the pseudo-SU_3 structure of the same type seen in the heavier, mother nuclei.* This is because the pseudo-SU_3 multiplet degeneracies $(2s+1)$ $(\tilde{N}-\tilde{n}_z+1)$ are very different at a given N of the mother nucleus and $\sim N/2$ in the going-to-be fragment nuclei (cf. ref. [2]; also [17]). Consequently, if we are able to observe the groups of neighboring hyperdeformed nuclei in accordance with the pseudo-SU_3 multiplet structure, cf., *e.g.*, ref. [18], as it was the case with the superdeformation, we will be able to decide whether such a structure is still present on the way to fission in the range of $\alpha_{20} \sim 1.0$–1.5 and thus *determine the natural limits of applicability of this symmetry in nuclei.*

There exists yet another fascinating physics motivation possibility that, even if difficult to identify today, is

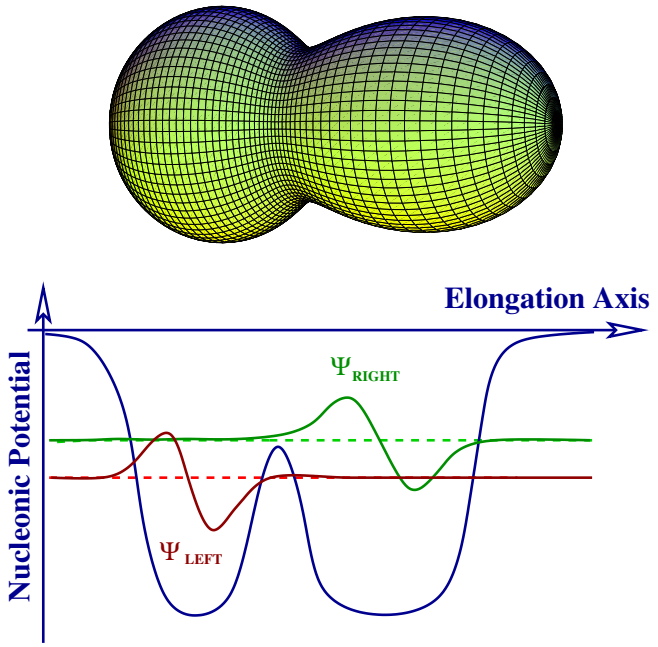

Fig. 4. When nuclei begin to form a "neck" the corresponding nuclear potentials react quickly by building up a barrier (calculations show that this mechanism is much stronger than what our intuition would typically tell us). In this type of shapes the term "axis ratio" *loses its meaning* given the fact that the neck radius tends to zero. (Strictly speaking there are up to six different semi-axes that can be defined in such a system.) At the same time, characteristic energy doublets (the large splitting here are out of proportion) are expected to emerge in a rather broad energy range close to the Fermi level. (The nuclear surface represented above corresponds to $\alpha_{20} = 1.1$ and $\alpha_{40} = 0.11$, superposed with a strong mass asymmetry.)

worth keeping in mind. When the nuclear elongation corresponding to the quadrupole deformation in the range of $\alpha_{20} \sim 1.1$–1.5 is *really* approached, the necking will develop, its size varying as a function of the nucleus and spin. In particular, the strong mass asymmetry can be expected if one of the going-to-be fragments is doubly magic (as ^{100}Sn for example). These going-to-be fragments related to a hyperdeformed configuration can be considered still strongly correlated; below, to simplify the language we will call them "fragments" in short, in contrast to the usual meaning of this word.

Single-particle energy "doublets" represented schematically in fig. 4 *are not* the energy doublets in the common sense: the corresponding wave functions are strongly localized in only one of the two going-to-be fragments and thus the discussed energy levels can be associated with one fragment at the time only. A doubly magic fragment will develop large spherical magic gaps; the other fragment will have a deformed, degeneracy-free single-particle spectrum. The presence of two, partially de-correlated single-particle spectra in one single mother nucleus is an extremely interesting physical situation as commented below.

Since the discussed elongations are so extreme (they exceed the elongations associated, *e.g.*, with the fission isomers in the actinide nuclei by up to a factor of two), the nuclear moments of inertia are huge and the implied rotational frequencies —relatively very low— even at very high angular momenta. The corresponding single-particle wave functions are "deformation aligned" and the single-particle Routhians nearly constant as a function of rotational frequency, except for the highest-j smallest-Ω content orbitals that align their spins with the axis of rotation directly at nearly vanishing frequencies.

As a result of the existence of two nearly de-correlated single-nucleon spectra in one mother nucleus and because of only relatively low rotational frequencies, the Coriolis (anti-pairing) mechanism will be strongly weakened. In nuclei at these conditions one should expect a *coexistence of the superfluid (deformed nucleus) and normal (spherical nucleus) phases in a single finite system.* This seems to be a unique physical situation also compared to the condensed-matter-physics standards. Its experimental manifestation could be analyzed in terms of model-dependent calculations that would involve comparison of the moments of inertia corresponding to a partly rigid partly superfluid system. In particular, the single-nucleon alignment properties promises to be very exotic: using the standard (although particularly incorrect in the case of hyperdeformation) convention of labeling the orbitals, an $m_{21/2}$ orbital corresponding to $\Omega = 1/2$ projection, diving under the Fermi level of a deformed fragment that can carry at most, say, $h_{9/2}$ orbitals, must undergo very unusual and thus fascinating transformations. There is a number of other appealing mechanisms that one may associate with those highly elongated systems; discussions of the related mechanisms are presently at a very early stage.

Let us mention that the "identical band mechanism" is also expected to be present at hyperdeformed configurations. In the case of the superdeformed nuclei, say A, and $A+1$, the relative polarization in terms of the moments of inertia, $\delta J/J$ (where $\delta J \equiv J(A+1) - J(A)$) was predicted to be a positive but decreasing function of the elongation, reaching zero at $\alpha_{20} \sim 0.6$ for the $n_z = 0$ orbitals. This quantity is expected to be negative at the hyperdeformation and the orbitals with $n_z = 1$ or 2 are expected to give nearly zero polarizations. (The predictions quoted are based on the mean-field calculations that employ the self-consistency condition: its experimental verification will be a precious message related to the self-consistency at the extreme nuclear elongation.)

4 Possibly decisive role of Jacobi transitions

The successful series of experiments that over many years has brought hundreds of superdeformed bands known today was in a way "quite easy": by reading the diagrams of the calculated single-particle levels and by finding the corresponding superdeformed gaps predicted by theory, *e.g.*, around ^{152}Dy, we were able to obtain the experimental information on nearly every bigger gap predicted. Let us discuss this aspect in some more detail.

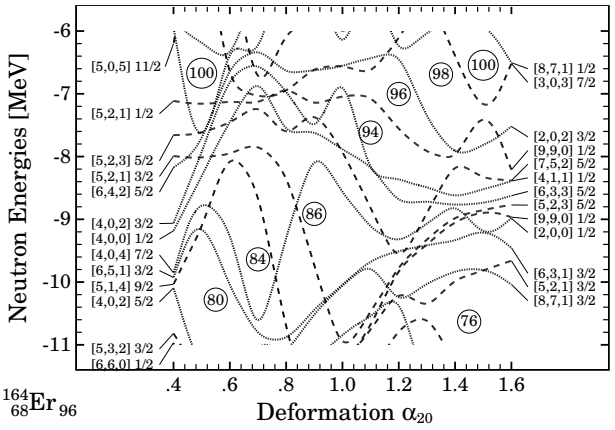

Fig. 5. Single-particle neutron levels at large deformations covering the super- and hyper-deformation ranges: here based on the deformed Woods-Saxon potential. (The diagram is characteristic for the relatively broad range of nuclei in the $A \sim 160$ mass region, including ^{152}Dy nucleus.)

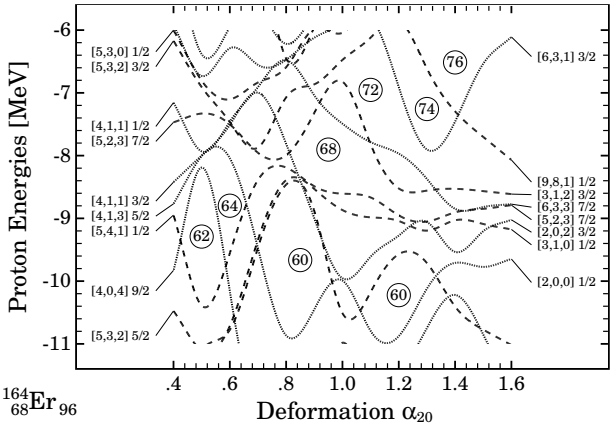

Fig. 6. Similar to the diagram in fig. 5 but for the protons.

4.1 Jacobi transition and super- and hyper-deformed states in ^{152}Dy

By inspecting the results in figs. 5 and 6 we can easily verify that there is not a very large difference between the gap sizes at the "traditionally" superdeformed and the hyperdeformed configurations. Similar conclusions hold for the protons.

In order to better understand the possible reasons for an "easy" success with the nucleus ^{152}Dy, let us recall that the high-spin nuclear states of interest in the present discussion are typically populated in the heavy-ion x-n reactions that produce, at the early stages of the process, highly excited compound nuclei with temperatures that easily exceed $T \sim 1.0$ MeV, a limit that according to theory corresponds to the melting of the deformed-shell structure. Consequently, we can learn about the behavior of *hot nuclei* at this stage of the reaction by examining the corresponding purely macroscopic-model energy. Such an analysis will be performed using a new version of the macroscopic model [19] called *Lublin-Strasbourg Drop* (referred to as LSD below).

We begin with the "standard" case: the nucleus ^{152}Dy, whose superdeformation, as well as the population properties, can be considered very well known. In particular, the highest-spin discrete transition of the yrast band in this nucleus corresponds to $I_{\max} \sim 64\hbar$.

Jacobi transition

Results in fig. 7 indicate that the equilibrium deformation in hot ^{152}Dy nucleus remains oblate and increases to about $\beta_2 \sim 0.28$ ($\gamma = 60°$) up to spin $\sim 68\hbar$. From that value on, when spin increases, the equilibrium deformation becomes triaxial and moves quickly towards high elongations. That process does not mean any complete loss of stability against fission, since the fission barriers are still rather high. The transformation that leads from oblate to triaxial and strongly elongated shapes when spin increases (or, from the elongated, towards the oblate equilibrium shapes when spin decreases) is usually called the nuclear Jacobi transition [16].

Spin window

An important implication of the above result is that if the ^{152}Dy nucleus is populated at spins corresponding roughly to the interval $[70, 78]\hbar$ (below we call this interval spin window), the corresponding population flux *must pass* through the large-deformation states and thus feeding of the superdeformation is the *dominating* population channel —but only within this (relatively narrow) spin window. Since the mother nuclei corresponding to, *e.g.*, a $4n$ reaction have similar spin window properties, we may conclude that the spin difference between the lower bound of the spin window and the spin associated to the first discrete transition observed is $\sim$ 6–8$\hbar$. This defines an average angular-momentum escape per evaporated nucleon $\sim$ 1.5–2$\hbar$, the latter estimate being in agreement with measurements for many other reactions in this nuclear range. We may expect that similar orders of magnitude will be preserved by the neutron evaporation from the hyperdeformed nuclei.

Neutron evaporation threshold

We have just emphasized the importance of the condition of a sufficiently high fission barrier at zero temperature and of the spin window related to the Jacobi transition; for the population of a hyperdeformed nucleus of interest it is of advantage if no further neutron evaporation is energetically possible. This condition is usually simplified by saying that fission barriers higher than $\sim$ 8 MeV (a typical order of magnitude for the neutron binding energy in the mass range $A \sim$ 150–170) are not contributing strongly to an increase in stability since the neutron evaporation channel open will in general render the mother nucleus not directly observable.

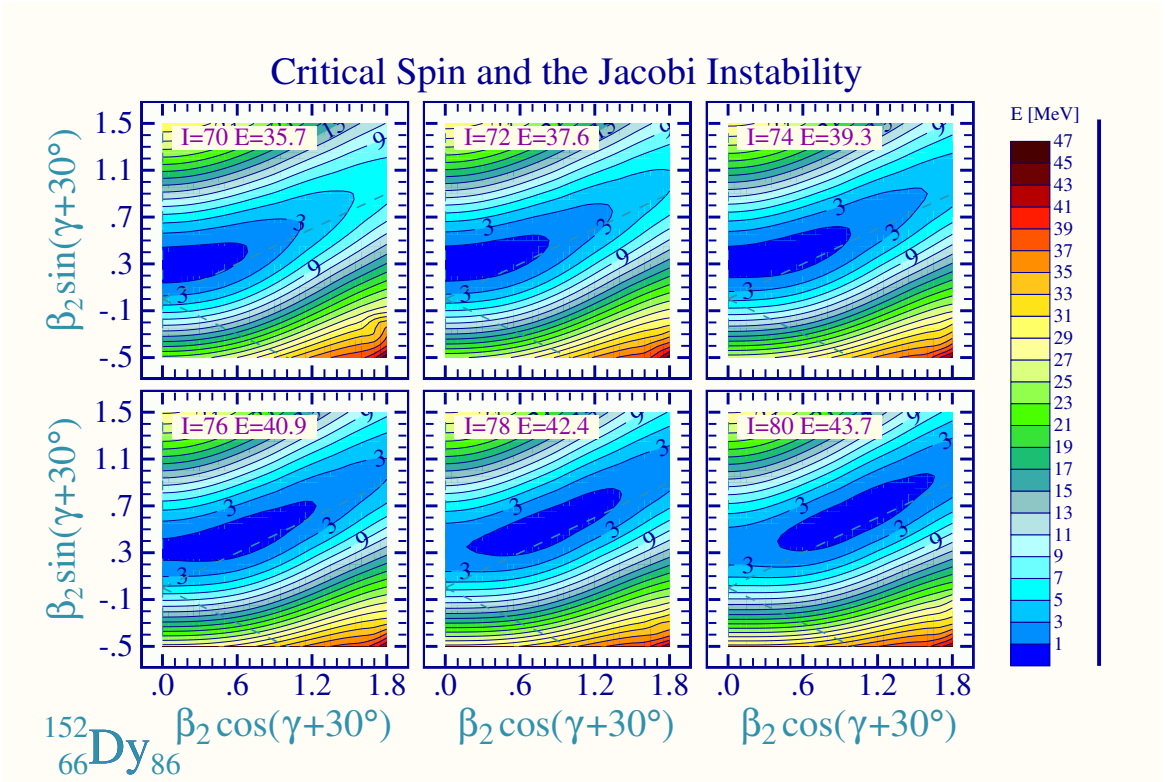

Fig. 7. Total-energy calculations in terms of the standard $(\beta - \gamma)$ deformations according to the LSD approach. At each spin and deformation point the energy was minimized with respect to α_{40}, α_{60} and α_{80}. It has been verified by a direct comparison with the full minimization variant of the code (whose results are presented and discussed also below) that these variables are sufficient to draw the conclusions of interest here. Each map is normalized separately to zero at the respective minimum, however, the true minimum energies (in MeV) are given in the boxes next to the spin values. Calculations correspond to the ^{152}Dy nucleus that clearly undergoes the Jacobi transition beginning with critical spin $I_{\rm cr} \sim 68$–$72\hbar$. From that critical range on, the equilibrium deformation moves quickly towards large elongations when spin increases, while the fission barrier, although decreasing, remains relatively high —and the corresponding nucleus relatively stable— with respect to fission.

Double-hump inner barrier

One can see from fig. 5 that relatively large $N = 86$ gaps exist not only at $\alpha_{20} \sim 0.6$, but also, after some level crossing visible in the figure, at $\alpha_{20} \sim 0.9$. This second $N = 86$ gap has been discussed earlier in the literature and was actually giving rise to the first mention of the hyperdeformation[2]. From the results in fig. 9, sect. 4.3, one can see that the minimum related to the $\alpha_{20} \sim 0.9$ deformation persists down to spins $I \sim 50$; yet the "left hyperdeformed barrier" (as opposed to fission barrier) has a double-hump structure with the deep superdeformed minimum lying to the left.

This double-hump structure in the barrier is most likely one of the reasons for the difficulties to observe the hyperdeformation in ^{152}Dy, mainly because the corresponding inner (left) barrier is, in relative terms, too small. More precisely, since all the large-deformation nuclear configurations are populated through the high-temperature stage, the cooling of the nucleus during the neutron evaporation process will cause the appearance of the deeper (superdeformed) minimum much earlier *i.e.* at higher residual temperatures, as compared to the hypothetical appearance of the shallower (hyperdeformed) minimum. Consequently, the high proportion of the population flux goes most likely to the superdeformed minimum, leaving the population rate of the hyperdeformed one beyond the todays instrumental sensitivity threshold.

The double-hump structure of the inner barriers is most likely one of the slowing-down factors in the search for the hyperdeformed minima in nuclei in which the superdeformation has already been experimentally confirmed.

[2] The possibility of the existence of the $\alpha_{20} \sim 0.9$ minimum in addition to the $\alpha_{20} \sim 0.6$ minimum was discussed by one of the authors (J.D.) at the 1987 *Nuclear Chemistry Gordon Conference*; at that time it was referred to as "*super-superdeformed*". The name "hyperdeformation" was suggested in the same context by Frank Stephens. The corresponding energy landscape obtained from the early calculations of that type has been adapted as one of the illustrations in the scientific motivation document related to GAMMASPHERE.

4.2 Hyperdeformed nuclei with and without Jacobi transition

From the results in figs. 5 and 6 we may expect that any combination of the proton numbers $Z = 68$ (70), 72–76 with the neutron numbers $N = 94$–100 suggests a good candidate nucleus for the hyperdeformation studies. Such

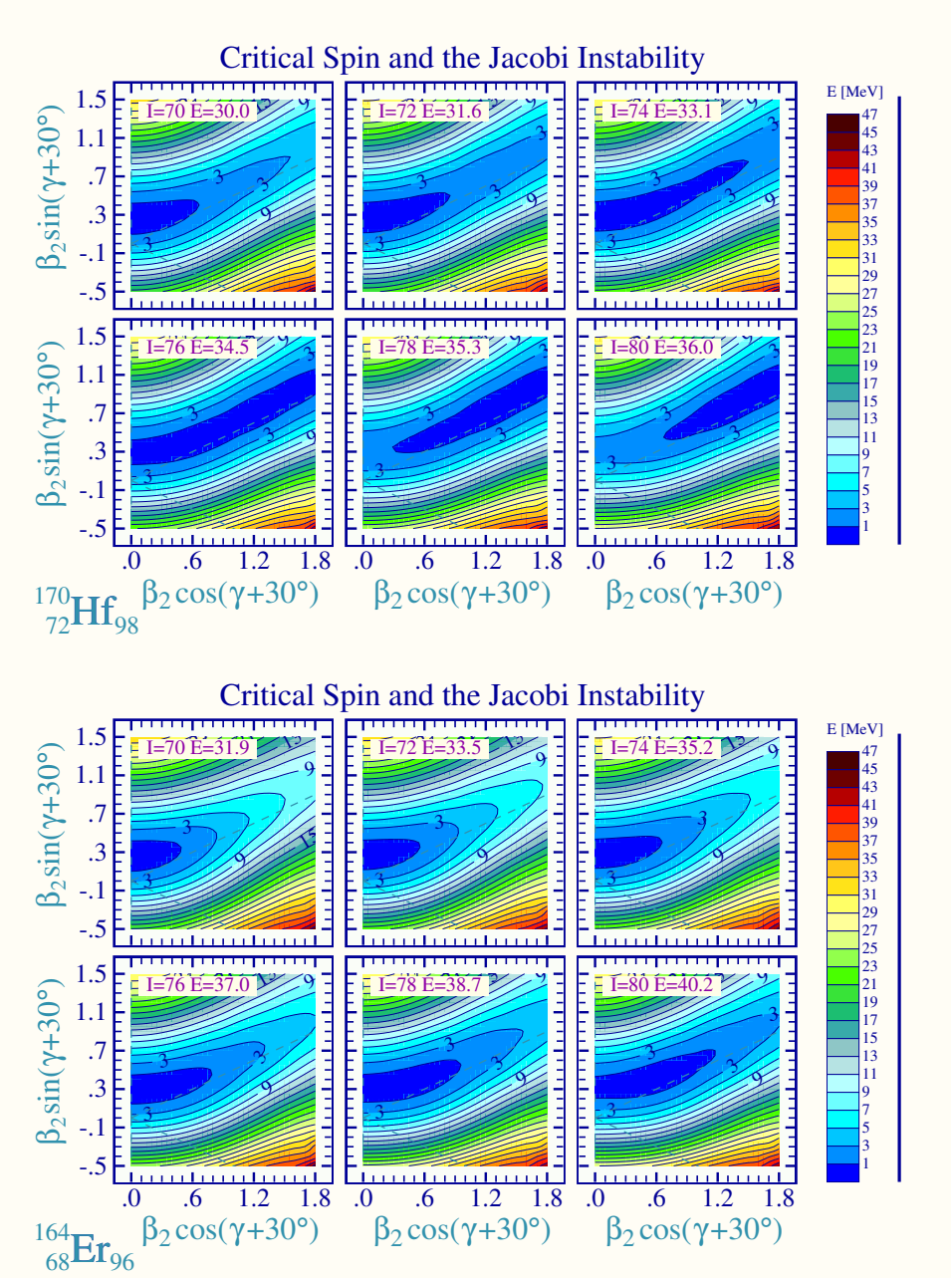

Fig. 8. The macroscopic-model calculations representative for the high-temperature nuclear behavior; here for ^{170}Hf (top) and ^{164}Er (bottom). The almost immediate loss of stability against fission already at the oblate deformation and the almost "instantaneous" Jacobi transition at fission barriers that are negligible make ^{170}Hf a nucleus not of the first choice. In contrast, the case of ^{164}Er seems to have an advantage: the latter nucleus undergoes a Jacobi transition and the population of the large deformations $\alpha_{20} \sim 0.8$–0.9 is likely since the fission barriers are markedly higher than zero in this case.

a statement would be based solely on the predictions related to the *zero-temperature* nuclear-stability condition that in turn relies exclusively on the corresponding shell closures. This "zero-temperature" criterion alone is not sufficient, as the unsuccessful searches for some hyperdeformed nuclei in the Er-Hf region have demonstrated. Moreover, as the discussion following results in fig. 7 suggests, it is most likely essential that the whole flux populating large-deformation states passes through the excited large-deformation intermediate states first of all at the high-temperature limit.

Comparison of the results in fig. 8 makes it clear that out of two nuclei predicted to have hyperdeformed minima at the zero-temperature limit, one may, and another one may not, manifest the Jacobi transition. In particular, it is seen from the figure that ^{164}Er does undergo a Jacobi transition and because of that should in principle be a candidate for an experiment. Whether the ^{164}Er barriers seen in fig. 8 are sufficiently high is not quite clear as long as no experimental confirmation exists but a similarity to the results for the ^{152}Dy case (cf. fig. 7) is suggestive.

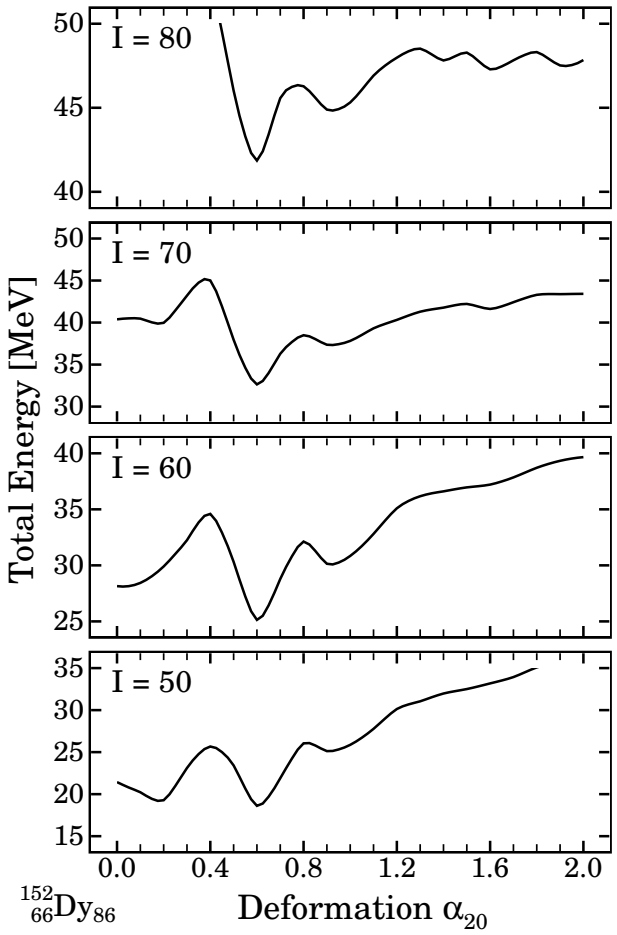

Fig. 9. Total-energy cuts using a new approach based on the Strutinsky method with the Dirac single-particle potential and the LSD macroscopic approach. The energy has been minimized with respect to α_{40}, α_{60} and α_{80} at each α_{20} value.

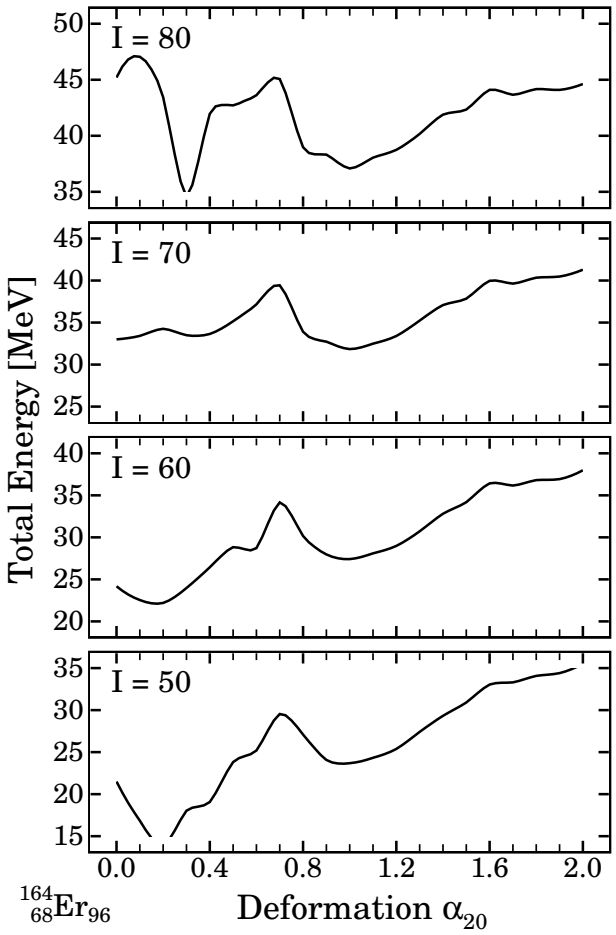

Fig. 10. Similar to fig. 9 but for the nucleus ^{164}Er. If this nucleus survives the high-temperature regime, its shell effects are predicted to be strong enough to produce relatively high barriers, both against fission and the inner one, down to the low-spin area. At the same time, the barriers do not have a double-hump structure as in the case of ^{152}Dy, fig. 9 (except around $I \sim 70$, where the yrast and the hyperdeformed minimum have comparable energies).

The results of the total-energy minimization seen in fig. 8 correspond to the maximum multipole number $\lambda=8$; with the number of multipoles extended up to $\lambda = 14$ the barriers become of course slightly lowered as compared to what one can read from the upper-right corners in the figure. In particular: for ^{164}Er, these more exact calculations give $B_{\rm f}(I = 68) = 10.1$ MeV, $B_{\rm f}(I = 74) = 5.4$ MeV and $B_{\rm f}(I = 80) = 2.0$ MeV; these heights correspond to the deformations that are out of the range of the figure.

In reference to the ^{164}Er example, let us mention that by increasing the neutron number one will also increase the fission barriers. This remark is important knowing that the envisagable compound nuclei leading to the one in question will necessarily have larger neutron numbers.

4.3 New microscopic calculations

The results discussed so far in this paper addressed principally two aspects of the theory: the existence (or not) of the deformed shell closures and the fission stability (or instability) at the relatively high-temperature limit.

The ultimate argument about the stability of a nucleus is always based on the microscopic calculations that take into account a sufficient number of the relevant degrees of freedom and allow to estimate the behavior of the total nuclear energy taking into account the quantum effects.

Here, we would like to present only a few examples of such calculations (cf. figs. 9-10) and report briefly on the new generation of the microscopic Strutinsky-type calculations that are based on the following elements.

Macroscopic energy

We have already mentioned the use of a new approach based on the LSD method [19] when discussing the Jacobi transitions. This improved approach allows to reproduce the experimentally known nuclear masses with the record-low r.m.s. deviations (cf. appendix). In addition, by taking into account the nuclear surface curvature effects, this

new approach allows at the same time for an increased precision in the fission barrier calculations. Both these elements encouraged us to apply it in the new generation of the Strutinsky calculations.

Mean field and its parameterization

In generating the single-particle Hamiltonian and energy levels a new approach based on the Dirac formalism with the deformed Woods-Saxon potentials has been developed. The parameters of the Hamiltonian have been adjusted to single-particle level positions in both spherical and deformed ("band heads") nuclei, to known nucleonic binding energies as well as r.m.s. radii and charge densities. We believe that by introducing the above up-to-date experimental information to the theoretical model we are able to provide a powerful phenomenological tool for the advanced large-scale calculations, ref. [20].

Pairing and the particle number projection

Within the hyperdeformed configurations and also at the surrounding deformations the high-spin states are usually characterized by a relatively low-frequency rotation. Consequently, the pairing correlations are not necessarily negligible and in the present approach they are taken into account "by default" using a particle number projection technique within the Bogolyubov transformation formalism.

Fast minimization algorithms

Usually, large-scale Strutinsky-type calculations have been performed by using a mesh of deformation points. It is, however, impossible to apply this technique in the case of large number of deformations such as five or more because of the computer limitations. In the case of high dimensionalities of the deformation space it is more of advantage to use directly the fast minimization routines that make the Strutinsky method resemble the functioning of the Hartree-Fock approaches.

Comparison of the results in figs. 9-10 shows that, consistently with the single-particle diagram predictions in figs. 5-6, the hyperdeformation in ^{164}Er is larger ($\alpha_{20} \sim 1.0$ compared to $\alpha_{20} \sim 0.8$ in the case of ^{152}Dy). Both barriers (*i.e.* the fission barrier and the inner barrier) in ^{164}Er are comparable to those in ^{152}Dy and the problem of populating the hyperdeformation in the former case seems to be related strongly to the possibility (or impossibility) of reaching the narrow spin window of $I \sim 74$–$78\hbar$ in the corresponding reaction (cf. fig. 8, bottom part) feeding the ^{164}Er nucleus.

Finally, let us mention that the example of ^{164}Er is by no means the only one worth considering in this mass range. However, what is worth emphasizing is the question of the existence of the Jacobi transition in the mother nucleus and in nuclei on the way to the final one during the process of particle evaporation.

5 Nuclei in the mass range A $\sim$ 100–120

As is known from the fission barrier systematics, the nuclei in the mass range $A \sim 100$–120 are characterized by relatively high barriers against fission and thus are expected to withstand better, in particular the high-spin rotation. An implication of such a property will be that, on the average, also larger deformations will be populated both in the intermediate stages of the reaction and possibly in the final one (if the shell structure conditions are favorable).

We begin by showing that in the discussed mass range the deformed-shell effects may indeed stabilize the nuclei at larger elongations which most likely opens new perspectives as argued below. It will be shown next that the Jacobi transition mechanism favors the population of deformations approaching $\alpha_{20} \sim 1.4$.

5.1 New nuclear states that possibly need a new name

We arrive at a situation that can be summarized as follows. Only with the nuclei that are most stable against fission we may hope to populate the $\alpha_{20} \sim 1.4$ deformations *i.e.* configurations with real[3] axis ratio 3 : 1. It will be instructive to study the corresponding shell structure in some details as presented in fig. 11.

Let us consider as an example the nucleus ^{108}Cd; since its proton number satisfies $20 < Z = 48 < 50$, the corresponding main shell at spherical shapes is $N^{\pi}_{\rm sph} = 3$ and according to the second definition of the hyperdeformation that has been quoted earlier, the associated hyperdeformed orbitals should originate from the shell $N^{\pi}_{\rm sph} = 6$. Similarly, since the neutron number in question satisfies $50 < N = 60 < 82$, the corresponding $N^{\nu}_{\rm sph} = 4$ and the associated hyperdeformed orbitals should originate from the shell $N^{\nu}_{\rm sph} = 7$. Inspection of fig. 11 indicates that there is at least one neutron orbital originating from the spherical shell $N^{\nu}_{\rm sph} = 8$ orbital expected to be occupied (!) while at the proton number $Z = 49$ there is also one proton orbital occupied that originates from the shell $N^{\pi}_{\rm sph} = 7$ (!!).

Such a situation has not been foreseen by the definitions of the hyperdeformation discussed earlier. One can see that the physical situation implied by the present discussion exceeds the earlier expectations since the downsloping orbitals coming from the $(N_{\rm sph} + 4)$-th shell were not discussed so far —wherefrom the question of the possible name of the new structures[4].

[3] Since the reference to the axis ratios 2 : 1 and 3 : 1 has been often confusing (*e.g.*, the nuclei with $\alpha_{20} \sim 0.9$, traditionally called "hyperdeformed —thus with the axis ratio 3 : 1" while in reality the corresponding elongation barely makes for 2 : 1, cf. fig. 3) we stress the fact that here we *really mean it:* the deformation in question is $\alpha_{20} \sim 1.4$, thus corresponding to the axis ratio 3 : 1.

[4] We have pointed out in a few places of this article to the conflicts associated with the unfortunate (mis)use of the axis ratio terminology. However, there is yet another conflict related to the names "superdeformation" and "hyperdeformation"

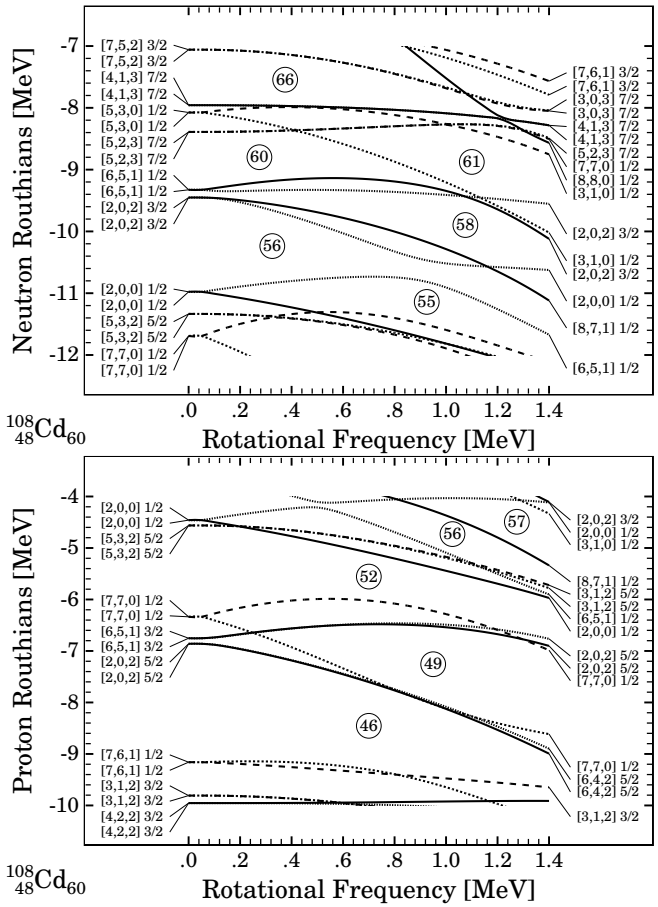

Fig. 11. Single-particle Routhians at $\alpha_{20} = 1.4$ and $\alpha_{40} = 0.3$ appropriate for the real 3 : 1 axis ratio (see the text).

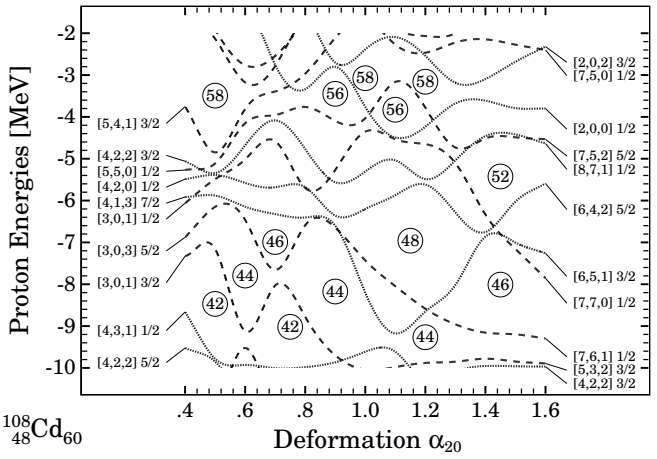

Fig. 12. Single-particle proton levels at the hyperdeformation and or megadeformation region with proton number ~ 40 nuclei. Huge shell effects (gaps that approach $\Delta E \sim 3$ MeV at $Z \sim 46$–48 at deformations $\alpha_{20} \sim 1.2$–1.4, thus the axis ratio not far from 3 : 1, cf. fig. 3), deserve attention.

One possibility would be to continue using the nomenclature originating from the Greek by either using the Greek word $\mu\varepsilon\gamma\alpha\sigma$ (megas) for "great" —wherefrom "megadeformed" for the exotic configurations discussed above, or using the Greek word $\gamma\iota\gamma\alpha\sigma$ (gigas) for "giant", wherefrom "gigadeformed" for the same. Since the scission configurations of many nuclei correspond to $\alpha_{20} \sim 4.0$ (in the fission barrier calculations extending to the nuclear scission points the α_{20} deformation is accompanied by several other non-zero multipoles) it would be safer to use the word megadeformation for the hypothetical $(N_{\rm sph} + 4)$-th shell configuration at $\alpha_{20} \sim 1.4$ (or the real 3 : 1 axis ratio) and reserve the word gigadeformation for any possible surprise when $\alpha_{20} \to 4.0$.

The nuclei corresponding to $N_{\rm sph} = 3$ are predicted to have the tendency to build up very strong hyperdeformed- and/or megadeformed-shell effects as fig. 12 illustrates. This tendency provides one more argument in favor of investigating the nuclei in the corresponding mass range.

themselves. Actually, the word "super" is the Latin version of the Greek preposition "hyper" (meaning "over" or "beyond"). Therefore, strictly speaking, the words "superdeformation" and "hyperdeformation" can be seen to express *the same thing* in two different languages [21].

5.2 Slow Jacobi transitions in A $\sim$ 100–120 range

We would like to show that in the discussed mass range the Jacobi transition mechanism indeed stabilizes the nuclei at larger elongations and most likely helps opening new perspectives as argued in the preceding sections. As can be seen from the results in fig. 13, deformations approaching $\alpha_{20} \sim 1.4$ could be fed while the fission barriers are still considerably high. Moreover, the spin windows corresponding to the transition in terms of the equilibrium deformations from $\gamma = 60^\circ$ down to fission are much larger in the lighter nuclei discussed here as compared to nuclei in the $A \sim 160$ mass range discussed earlier in this paper.

This large size of the spin window, referred to as a slow Jacobi transition, is clearly a factor that facilitates thinking of a more efficient population of these exotic structures by experiment. It is usually difficult to satisfy the high-angular-momentum transfer condition when it is limited to a very narrow spin window of a few $\hbar$ only, as it is usually the case in the heavy-mass nuclei. We believe that the presence of the *very narrow* spin window that implies such a restrictive population conditions was "overlooked" at least in some experimental attempts undertaken so far in this domain.

Moreover, with the nuclear deformation range that approaches experimentally the *real* 3 : 1 axis ratio configurations, the giant-dipole resonance radiation should move considerably low in energy, the 4–6 MeV interval for its lower shoulder being the range to think of. This may imply that experiments prepared for the high-energy gamma-ray analysis will have a better chance to observe the huge deformations —if not through discrete— through continuous electromagnetic transitions.

Last but not least, with the *real* 3 : 1 axis ratio configurations populated the asymmetry in the Coulomb barriers should clearly favor the proton emission from the "tips of the nuclear cigar" and the use of the charged-particle

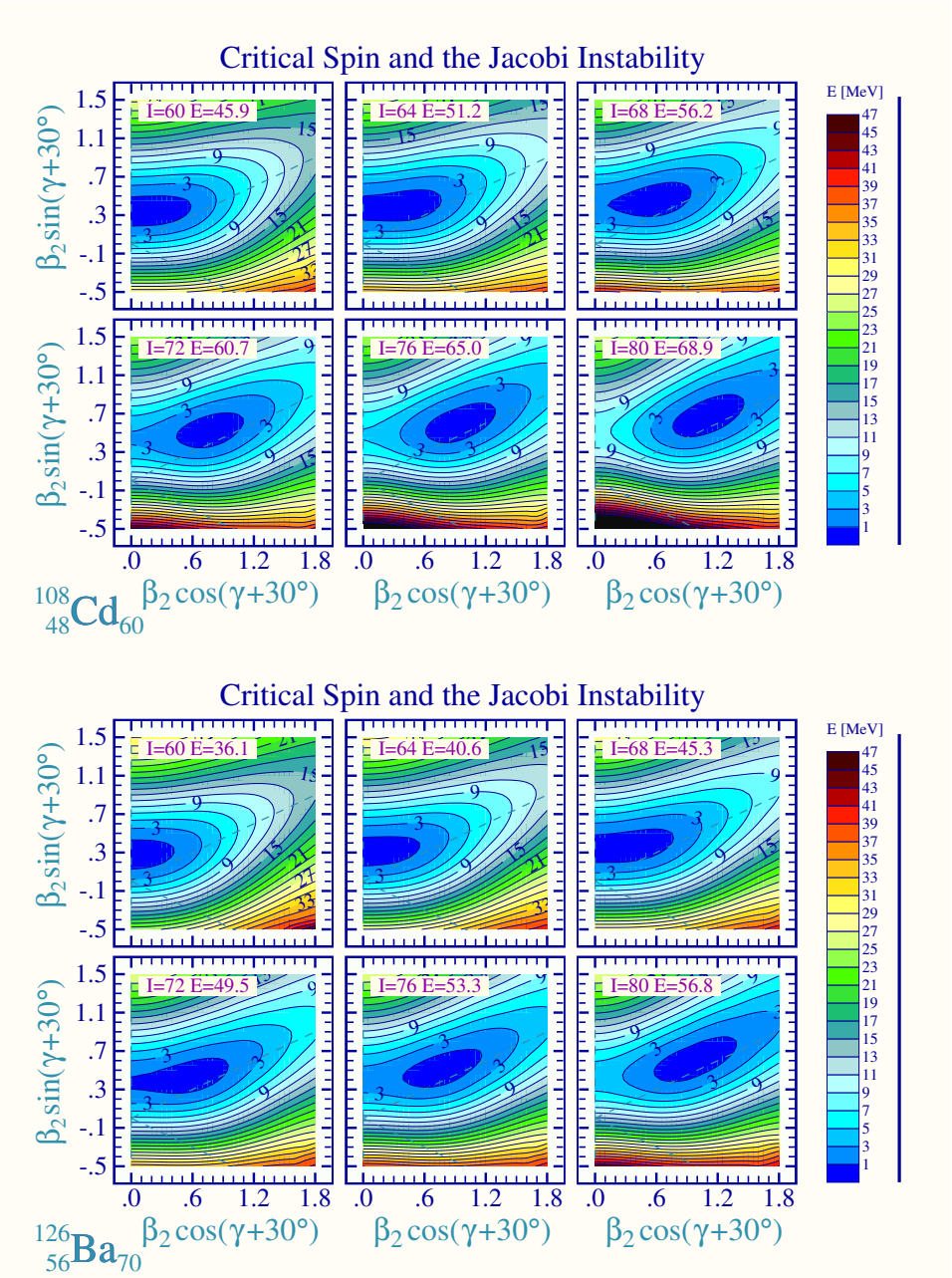

Fig. 13. The Jacobi transition representations for ^{108}Cd and ^{126}Ba nuclei. The former has recently been studied, ref. [22], the latter will be studied shortly within the EUROBALL Collaboration, ref. [23].

auxiliary detectors (if possible as a routine) may increase the chances of enhancement of the processes that for many years remained so difficult to observe.

We may conclude that the population of very large deformations in hot nuclei in the mass range $A \sim 100$–120, a prerequisite when searching for the hyperdeformed (and perhaps megadeformed) nuclear configurations in this mass range should be enhanced owing to the particularly extended form of the Jacobi transitions as predicted for the nuclei in question.

5.3 Nuclei in the vicinity of barium

Below we are going to illustrate some theoretical results for the ^{126}Ba nucleus that was receiving recently a significant attention within the EUROBALL Collaboration. This nucleus is expected to undergo a Jacobi instability that extends over a relatively broad range of spins and thus should be considered as a good candidate for the *gigantic back-bending* and possibly also for the hyperdeformation studies.

The shell effects examined systematically in the earlier calculations such as ref. [24] indicate that the strong hyperdeformed-shell closures in rotating nuclei are to be expected in medium heavy ($A \sim 160$) and heavy ($A \sim$ 180–210) nuclei. Those early calculations did not give any special indication for the particularly strong hyperdeformation shell effects in the lighter-mass nuclei, but they were based on the relatively limited deformation space,

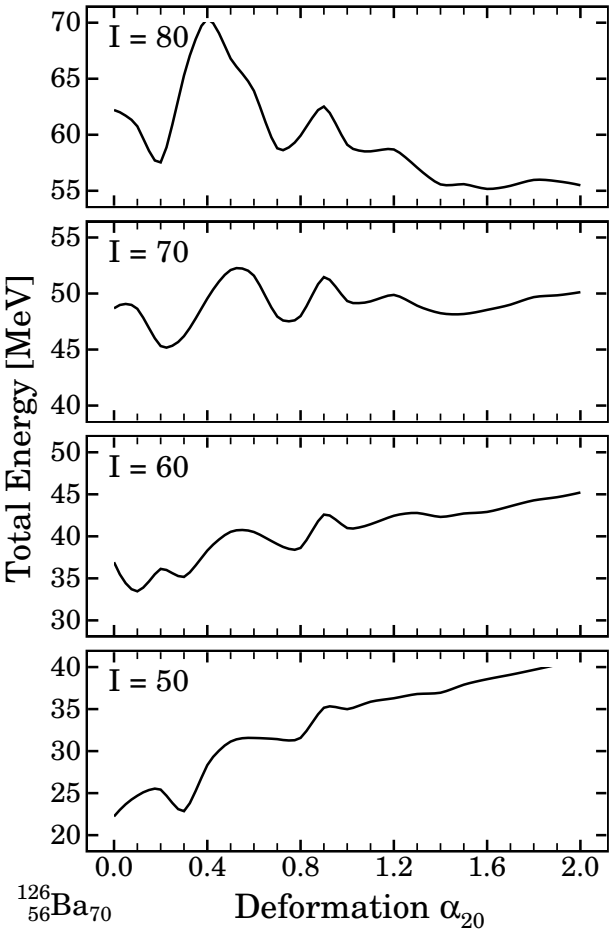

Fig. 14. Similar to fig. 9 but for the nucleus ^{126}Ba; cf. also pure LSD energy minimization curves in fig. 15.

so that revisiting this nuclear range with more sophisticated theoretical means seems appropriate. Results in fig. 14 obtained as previously by minimizing the total nuclear energy at each quadrupole deformation over α_{40}, α_{60} and α_{80}, indicate that a large-deformation minimum may build up at the spin range $I \sim 60$–80; such a minimum, if populated, should give rise to about a dozen of discrete quadrupole transitions.

6 Conclusions: possibly setting new priorities

We have studied and discussed the possibilities of populating and observing the nuclear states with very large deformations at high spins. We have presented a selection of expected properties of the hyperdeformed nuclei and compared them, when possible, to the corresponding properties of the superdeformed ones.

We believe that the fact that some hot nuclei fission starting directly from the relatively small oblate equilibrium deformations was an important hindering factor at least in some experimental searches for the hyperdeformed nuclei in the $A \sim 160$ mass range. In contrast, some other nuclei in the same mass range may undergo the Jacobi transition, remain strongly deformed and at the same time relatively stable against fission. These nuclei are expected to be the candidates for hopefully more successful observation of the very large-deformation shapes. Although the existence of the Jacobi transition mechanism in nuclei has been known for a long time, to our knowledge, it has often not been taken into account when selecting the beam-target combinations for the experimental tests.

On the basis of the nuclear Jacobi instability properties in various mass ranges we have formulated a suggestion that hyperdeformed nuclei, whose nucleons occupy the orbitals from the $(N_{\rm sph}+3)$-rd, shell may not be the last ones on the large-deformation search agenda. According to theory, the nuclei in, *e.g.*, the $A \sim 100$ range seem to satisfy three important criteria:

1) They manifest strong shell gaps of about 3 MeV (!) at deformations of $\alpha_{20} \sim 1.2$–1.4.
2) They follow a slow Jacobi transition that favors populating the corresponding structures at high temperatures and simultaneously at relatively broad spin window.
3) Some nucleons there may occupy the orbitals originating from the spherical $(N_{\rm sph}+4)$-th shell —thus giving rise to the possible *megadeformed* states.

On the one hand, it may not sound very realistic suggesting a search for the megadeformation knowing that no hyperdeformed nucleus has been seen in discrete transitions so far. On the other hand, it is not true that the search difficulties increase proportionally to the nuclear elongation. In fact, what is needed are sufficiently "strong" potential barriers against fission and simultaneously against the return to the weaker-deformed configurations. Such conditions are not necessarily correlated with the actual size of the deformation in question; there may generally appear groups of megadeformed nuclei that are more stable than a group of the theoretically predicted hyperdeformed ones. (At present, we are studying such a possibility in more detail by performing microscopic calculations, but a precise comparison is not available to us at this time).

On the average, the shell effects corresponding to hyper- or mega-deformed shapes are for various reasons weaker than those at the superdeformed shapes. One of them is that the onset of the narrow-neck configurations may cause the disappearance of the pseudo-SU_3 multiplet structure that is known to help stabilizing the superdeformed shapes. Consequently, it may be an easier tactics to optimise the experiments for the continuous gamma-radiation searches for the hyperdeformed states rather than attempting the discrete-line studies by all means.

Moreover, the huge elongations in question must leave traces in terms of the low-energy shoulders of the giant resonances and at the same time in terms of the enhanced proton emission from the nuclear tips. This implies once again that the continuum gamma-ray studies combined with the detection of the light-particle emission may bring a successful identification of the hyperdeformed nuclei *via* the giant-resonance mechanism and/or a gigantic backbending mechanism in the continuum rather than a direct

observation of the equidistant gamma-rays that resemble the well-known superdeformation spectra.

Finally, let us mention that we have undertaken an effort trying to remove a confusion that has accumulated over the years in relation to the incorrect use of the so-called 2 : 1 and 3 : 1 axis ratio arguments/criteria. These arguments have been originally introduced on the basis of the harmonic-oscillator properties but were not confirmed by experiment. In particular, the superdeformed nuclei in the ^{152}Dy region that are characterized by the deformations $\alpha_{20} \sim 0.6$ and $\alpha_{40} \sim 0.1$ (or smaller) have the longer-to-shorter axis ratios of the order of 1.7. The nuclei expected to have $\alpha_{20} \sim 0.9$ and traditionally referred to as hyperdeformed have, in reality, the corresponding axis ratio 2 : 1.

On the occasion of this discussion, a more consistent way of naming the highly elongated nuclear configurations has been proposed.

Work supported in part by the Polish Committee for Scientific Research (KBN), grant No. 2 P03B 115 19, and by the Scientific Exchange Programme between IN2P3, France, and Polish Nuclear Physics Laboratories.

Appendix A. Liquid-drop mass formula with curvature term (LSD method)

The nuclear Liquid-Drop Model (LDM) was recently revisited, ref. [19]. The point the most relevant in the context of the present article consisted in extending the LDM of Myers and Świątecki by adding the surface curvature term. Earlier in the text this extended version of the model has been referred to as Lublin-Strasbourg Drop (LSD) approach.

According to the usual rules of the macroscopic energy models the LSD energy expression assumes that the mass of an atom with Z protons, Z electrons and N neutrons is described by the relation (cf. refs. [25,26]):

$$\begin{aligned} M(Z,N;\mathrm{def}) &= ZM_{\mathrm{H}} + NM_{\mathrm{n}} - 0.00001433\,Z^{2.39} \\ &+ b_{\mathrm{vol}}\ (1-\kappa_{\mathrm{vol}}\,I^2\,)\,A \\ &+ b_{\mathrm{surf}}\,(1-\kappa_{\mathrm{surf}}I^2\,)\,A^{2/3}B_{\mathrm{surf}}(\mathrm{def}) \\ &+ b_{\mathrm{cur}}\ (1-\kappa_{\mathrm{cur}}\,I^2\,)\,A^{1/3}B_{\mathrm{cur}}(\mathrm{def}) \\ &+ \frac{3}{5}\,e^2\frac{Z^2}{r_0^{\mathrm{ch}}A^{1/3}}\,B_{\mathrm{Coul}}(\mathrm{def}) - C_4\frac{Z^2}{A} \\ &+ E_{\mathrm{micr}}(Z,N;\mathrm{def}) + E_{\mathrm{cong}}(Z,N)\,, \end{aligned} \tag{A.1}$$

where

$$E_{\mathrm{micr}} = E_{\mathrm{pair}} + E_{\mathrm{shell}} \tag{A.2}$$

is the sum of the microscopic shell and pairing energies, while the terms proportional to $Z^{2.39}$ and to Z^2/A describe, on the average, the binding energy of electrons and the correction due to the surface diffuseness of the charge distribution, respectively. The LSD energy expression contains the congruence energy according to ref. [26]:

$$E_{\mathrm{cong}} = -10\,\mathrm{MeV}\cdot\exp(-42\,|I|/10)\,. \tag{A.3}$$

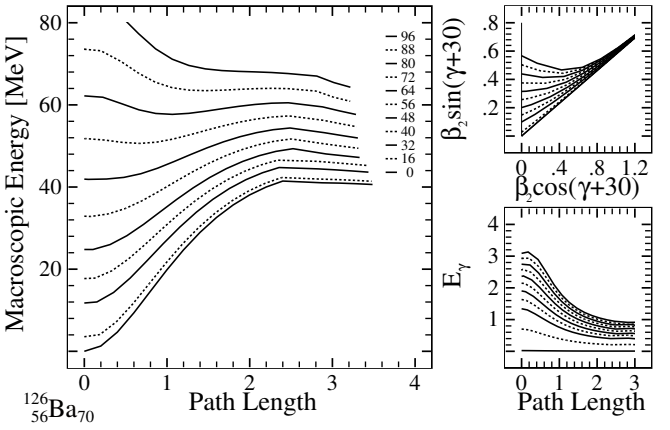

Fig. 15. The macroscopic energy according to the LSD approach minimized with respect to γ-deformation and the α_{40}-to-$\alpha_{14,0}$ even-multipolarity deformations at each quadrupole-deformation point as a function of the path length on the (β,γ)-plane for ^{126}Ba (left). The trajectories connecting the lowest-energy points at the oblate deformation, *i.e.* at $\gamma = 60^\circ$ and the scission points are shown in the upper-right-corner diagram. The rotational energies corresponding to the estimation $E_\gamma = \frac{\hbar^2}{2\mathcal{J}}\,[4I+6]$ calculated along each trajectory at spins $I = 16, 32, 40, 48, \ \ldots\ 96$ are shown in the lower-right-corner diagram.

The parameters of the LSD model were fitted to the 2766 known experimental masses, ref. [27], of nuclei with $Z > 8$ and $N > 8$ with the result

$$\begin{aligned} b_{\mathrm{vol}} &= -15.4920\ \mathrm{MeV} \\ \kappa_{\mathrm{vol}} &= 1.8601, \\ b_{\mathrm{surf}} &= 16.9707\ \mathrm{MeV}, \\ \kappa_{\mathrm{surf}} &= 2.2938, \\ b_{\mathrm{cur}} &= 3.8602\ \mathrm{MeV}, \\ \kappa_{\mathrm{cur}} &= -2.3764, \\ r_0^{\mathrm{ch}} &= 1.21725\ \mathrm{fm}, \\ C_4 &= 0.9181\ \mathrm{MeV}. \end{aligned}$$

The resulting mean square deviation for the binding energies $\langle\delta B\rangle = 0.698$ MeV, while for the fission barriers $\langle\delta V_B\rangle = 0.88$ MeV when the data for four nuclei with $A < 100$ are disregarded (the published results on the experimentally established fission barriers concern about 40 nuclei). These four nuclei, for details see ref. [19], pose difficulties to all models; the difficulties in question are attributed to the congruence effects that, however, escape the framework of the liquid-drop model. The traditional (*i.e.* without the curvature terms) liquid-drop model energy expression with the parameters adjusted to the experimental masses only, reproduces well the masses but gives fission barrier heights about 3 to 15 MeV higher than their measured values [19].

Within the LSD formulation no additional fit to the fission barriers has been performed; a very good description of the experimental fission barriers within the model obtained by fitting the masses only signifies an inner

consistency of the whole approach. In fact, the experimental binding energies and the fission barrier heights are reproduced with an accuracy comparable to or better than the Thomas-Fermi model of ref. [26], or the HF+BCS model with Skyrme forces of ref. [28].

Finally, it has been verified that the LSD approach offers a very high stability in terms of the extrapolation from the narrower range of nuclides to a more extended one —a property of particular interest when the information concerning unknown nuclei is sought.

We limit the illustration of the LSD calculation results to an overview of the high-spin behavior of the ^{126}Ba nucleus corresponding to the minimization of the LSD model energies over the even-λ multipole deformations $\alpha_{\lambda 0}$ up to $\lambda_{\max} = 14$, fig. 15. It can be seen from the figure that according to the calculations the Jacobi transition begins at $I \sim 70\hbar$ while the fission barrier disappears about $I = 88\hbar$. The corresponding minimum-energy trajectories connecting the minimum-energy points at an oblate deformation axis and the scission points are shown in the upper-right inset. The gamma-transitions energy at the spin values indicated, calculated along the same trajectories, are shown in the lower-right inset. We do hope that this information could be soon verified against the experimental results on ^{126}Ba obtained within the EUROBALL Collaboration.

Recently, another application of the LSD calculations to the ^{46}Ti study of large deformations and the giant-resonance features has turned out to be encouraging [29].

References

1. P.J. Twin *et al.*, Phys. Rev. Lett. **57**, 811 (1986).
2. J. Dudek, W. Nazarewicz, Z. Szymański, G. Leander, Phys. Rev. Lett. **59**, 1405 (1987).
3. R.V.F. Janssens, T.L. Khoo, Annu. Rev. Nucl. Part. Sci. **41**, 321 (1991).
4. J.F. Sharpey-Schafer, Prog. Part. Nucl. Phys. **28**, 187 (1992).
5. C. Baktash, B. Haas, W. Nazarewicz, Annu. Rev. Nucl. Part. Sci. **45**, 485 (1995).
6. I. Ragnarsson *et al.*, Phys. Rep. C **45**, 1 (1978).
7. B. Singh, R. Zywina, R.B. Firestone, Nucl. Data Sheets **97**, 241 (2002), available at: `http://www.nndc.bnl.gov/nndc/superdeformed/`.
8. H. Savajols *et al.*, Phys. Rev. Lett. **76**, 4480 (1996).
9. N. El Aouad *et al.*, Nucl. Phys. A **676**, 155 (2000).
10. W. Satula, J. Dobaczewski, J. Dudek, W. Nazarewicz, Phys. Rev. Lett. **77**, 5182 (1996).
11. J. Dudek, W. Nazarewicz, Phys. Rev. C **31**, 298 (1985).
12. T. Byrski *et al.*, Phys. Rev. Lett. **64**, 1650 (1990).
13. L.B. Karlsson, I. Ragnarsson, S. Aberg, Phys. Lett. B **416**, 16 (1998).
14. P. Fallon *et al.*, Phys. Rev. C **60**, 044301 (1999).
15. A. Galindo-Uribari *et al.*, Phys. Rev. Lett. **71**, 231 (1993); D.R. LaFosse *et al.*, Phys. Rev. C **54**, 1585 (1996); J.N. Wilson *et al.*, Phys. Rev. C **56**, 2502 (1997); V. Rizzi *et al.*, Eur. Phys. J. A **7**, 299 (2000).
16. S. Cohen, F. Plasil, W.J. Swiatecki, Ann. Phys. (N.Y.) **82**, 557 (1974).
17. J. Dudek, *Proceedings of the International Winter Meeting on Nuclear Physics, Bormio, Italy, 1987*, Ricerca Scientifica ed Educazione Permanente, Supplemento N. **56**, edited by I. Iori (Università degli Studi di Milano, Milano, 1987) p. 554.
18. J. Dudek, T. Werner, L.L. Riedinger, Phys. Lett. B **211**, 252 (1988).
19. K. Pomorski, J. Dudek, Phys. Rev. C **67**, 044316 (2003) nucl-th/0205011.
20. N. Schunck, PhD. Thesis, University of Strasbourg, avalilable at `http://tel.ccsd.cnrs.fr/view-thes-phys-theo_fr.html`.
21. The authors are indebted to C.A. Kalfas for turning their attention to this aspect.
22. A. Gorgen *et al.*, Phys. Rev. C **56**, 027302 (2002).
23. B. Herskind, private communication.
24. T. Werner, J. Dudek, At. Data Nucl. Data Tables **50**, 179 (1992); **59**, 1 (1995).
25. W.D. Myers, W.J. Świątecki, Ark. Phys. **36** (1967) 343; Nucl. Phys. **81** (1966) 1.
26. W.D. Myers, W.J. Świątecki, Nucl.Phys. A **601**, 141 (1996).
27. M. Antony, *Nuclide Chart 2002*, Impressions François, 103 Route de Marienthal, Haguenau, France; e-mail: `ela.myelin@ires.in2p3.fr`.
28. F. Tondeur, S. Goriely, J.M. Pearson, M. Onsi, Phys. Rev. C **62**, 024308 (2000); S. Goriely, J.M. Pearson, F. Tondeur, At. Data Nucl. Data Tables **77**, 311 (2001).
29. A. Maj *et al.*, this issue, p. 165.